

# DEHYDRATOR: Enhancing Provenance Graph Storage via Hierarchical Encoding and Sequence Generation

Jie Ying, Tiantian Zhu\*, Mingqi Lv, Tieming Chen

**Abstract**—As the scope and impact of cyber threats have expanded, analysts utilize audit logs to hunt threats and investigate attacks. The provenance graphs constructed from kernel logs are increasingly considered as an ideal data source due to their powerful semantic expression and attack historic correlation ability. However, storing provenance graphs with traditional databases faces the challenge of high storage overhead, given the high frequency of kernel events and the persistence of attacks. To address this, we propose DEHYDRATOR, an efficient provenance graph storage system. For the logs generated by auditing frameworks, DEHYDRATOR uses field mapping encoding to filter field-level redundancy, hierarchical encoding to filter structure-level redundancy, and finally learns a deep neural network to support batch querying. We have conducted evaluations on seven datasets totaling over one billion log entries. Experimental results show that DEHYDRATOR reduces the storage space by 84.55%. DEHYDRATOR is  $7.36 \times$  more efficient than PostgreSQL,  $7.16 \times$  than Neo4j, and  $16.17 \times$  than Leonard (the work most closely related to DEHYDRATOR, published at Usenix Security’23).

**Index Terms**—Advanced Persistent Threat, Provenance Graph Storage.

## I. INTRODUCTION

With the rapid increase in the scale and complexity of cyberspace over the past decade, cybercrime has grown correspondingly, much like a shadow. As of May 2024, there have been 9,478 disclosed data breaches [1]. Among these, the massive mother of all breaches (MOAB) in January 2024 stands out, with a staggering 26 billion records leaked, including information from platforms such as LinkedIn, Twitter, Weibo, and Tencent [2]. Sophisticated and well-funded threat groups seem to demonstrate the ability to infiltrate networks seemingly at will [3], [4], [5], [6], leading to a focus on audit logs to resist post-penetration [7]. Auditing is one of the fundamental guarantees of operating system security [8]. It is considered an essential condition for detecting vulnerabilities and penetration attempts in any resource-sharing system [9] and is identified as one of the three pillars of the “Gold Standard” of access control [10].

More and more evidence suggests that understanding the historical context of attacks through audit logs is crucial for attack hunting and causality analysis [11], [12], [13], [14], [15]. Provenance graphs constructed from kernel logs are increasingly regarded as an ideal data source for conducting

attack investigation due to their powerful semantic expression and attack historic correlation ability [16], [7]. Specifically, a provenance graph is a directed graph structure in which nodes represent system entities (e.g., process, file, and socket) and edges represent system-level events between entities (e.g., write, read, and fork). Provenance tracers continuously capture kernel logs through mature auditing systems to construct corresponding provenance graphs. Then they perform multiple queries on the provenance graph using specific algorithms to hunt potential threats, identify entry points, and determine attacks’s impact [17], [18], [19], [20], [21], [22].

To support these functions, a foundational infrastructure layer responsible for the storage of provenance graphs is essential. This layer must ensure accessibility for upper-layer components. However, four phenomena exist that cause difficulties in storing provenance graphs. (1) Irreversible Growth: To maintain data integrity, provenance tracers only add new data without deleting the existing data [23], [24]. This inevitably leads to the continuous expansion of the provenance graph. (2) Rapid Expansion: Due to the complexity of functionalities and the frequency of interactions, auditing frameworks generate a vast amount of kernel logs, with logs exceeding gigabytes per day on a single machine [25], [26]. (3) Extended Period: Cyber intrusions targeting government and enterprise systems can persist for extended periods. According to an industry report by TrustWave, the average duration of an intrusion before detection exceeds 188 days [27]. The three phenomena above result in intolerable storage costs for enterprises and security vendors attempting to centralize the construction of provenance graphs for threat hunting and causality analysis.

To address the challenge above, many studies start from an intuitive question: *how to store the same provenance graph in a smaller space?* We refer to all efforts aimed at solving this problem as **Efficient Storage Systems for Provenance Graphs (ESSPGs)**. Methodologically, we categorize existing ESSPGs into two types: Pruning-based and Encoding-based.

**Pruning-based ESSPGs:** This type of approach involves pruning parts of the provenance graph based on heuristic rules. LogGC [28] identifies and deletes events related to temporary and dead nodes, as they do not affect the system state and are useless for causality analysis. CPR [29] eliminates redundant events between source and target nodes by testing *interleaved flows*, i.e., whether any new inputs have been received at the source between the two system calls. NodeMerge [30] observes that globally read-only files are ineffective for causality analysis and removes events related to these nodes. DPR [31] retains only the necessary events for correctly traversing each entity’s ancestors (S-DPR) or both ancestors and successors (F-DPR), resulting in a reduced provenance graph. *However, these methods are lossy.* Although they claim that the pruning

This work is supported by the following grants: National Natural Science Foundation of China under Grant No. U22B2028 and 62372410. The Fundamental Research Funds for the Provincial Universities of Zhejiang under Grant No. RF-A2023009. Zhejiang Provincial Natural Science Foundation of China under Grant No. LZ23F020011.

J. Ying, T. Zhu\*, M. Lv, and T. Chen are with the College of Computer Science and Technology, Zhejiang University of Technology, Hangzhou 310023, China. E-mail: jieying@zjut.edu.cn, ttzhu@zjut.edu.cn\*, mingqilv@zjut.edu.cn, tmchen@zjut.edu.cn. \*corresponding author

does not affect upper-layer components, they cannot guarantee that every task will yield correct results. For example, ransomware detection heavily relies on the I/O operations of processes on files, but these events may be considered redundant and thus removed. Therefore, *pruning-based ESSPGs can potentially increase false negatives in the upper-layer components (e.g., threat hunting and causality analysis)*.

**Encoding-based ESSPGs:** This type of approach represents provenance graphs in a compact encoded form. Compression algorithms, such as Gzip [32] and DeepZip [33], compress the whole graph as a single file. This approach significantly reduces storage space but cannot support the query requirement of upper-layer components. Graph databases [34], [35], [36] store entity and event information in node and edge tables to support queries. Still, they do not consider the specific characteristics of provenance graphs, resulting in limited storage space reduction. SEAL [37] merges repeated fields of events to reduce the storage cost of timestamps. SLEUTH [38] combines encoding techniques, indexed table reference methods, and relative incremental representations, achieving an average storage overhead of only 10 bytes per event. However, the decompression time overhead is insufficient to meet the high demand for queries in causality analysis (e.g., returning the reverse provenance graph for a given point of interest). ELISE [39] and Leonard [40] combine high-frequency field mapping encoding with deep neural networks (DNN) to store log information. However, their auxiliary components (i.e., calibration tables) take up a lot of storage space thus undermining the objective.

To support the upper-layer components, we identify three key dimensions of ESSPGs within the infrastructure layer (provenance graph storage) from a large body of work in this line of research: (1) **Content-lossless**, which preserves all data in the provenance graph to avoid leading false negatives in upper-layer components; (2) **Storage-efficient**, which stores the original provenance graph with minimal storage overhead; (3) **Query-support**, which handles large-scale query demands from upper-layer components. However, *existing methods fail to satisfy these three requirements simultaneously*.

We propose DEHYDRATOR, a provenance graph storage system designed to meet the three requirements mentioned above. First, DEHYDRATOR extracts feature information (e.g., unique identifiers and entity names) and structural information (e.g., interactions between entities and timestamps) from the kernel logs collected by the audit framework to construct the provenance graph. This information is stored in the form of node tables and edge tables. Next, DEHYDRATOR constructs indexes on the redundant values in fields and replaces them, i.e., field mapping encoding. Then, we observe that causality analysis is an iterative process of querying incoming edges of nodes. Therefore, we treat the provenance graph as a layered directed graph and perform hierarchical encoding. Specifically, DEHYDRATOR uses a compact encoding form to store all incoming edge information for a node. Finally, we model querying as a sequence generation task, where the upper-layer component provides input information (e.g., node unique identifier) and returns the corresponding information sequence. This type of task is common in the NLP field.

Thus, DEHYDRATOR uses DNNs to memorize provenance graph information and constructs error-correction tables to counteract model misprediction. The detailed background and key insights into our design of these mechanisms can be found in Section II.

For the logs generated by the auditing framework, DEHYDRATOR uses field mapping encoding to filter field-level redundancy, hierarchical encoding to filter structure-level redundancy, and finally learns DNN to support batch queries. We evaluated DEHYDRATOR on seven datasets totaling over one billion logs. Experimental results show that DEHYDRATOR reduces the storage space by 84.55%. The storage efficiency of DEHYDRATOR is  $7.36 \times$  higher than PostgreSQL,  $7.16 \times$  higher than Neo4j, and  $16.17 \times$  higher than Leonard.

In summary, we make the following contributions:

- We propose DEHYDRATOR, an efficient provenance graph storage system that overcomes the limitations of existing methods and provides effective storage and querying. DEHYDRATOR uses field mapping encoding to filter field-level redundancy, hierarchical encoding to filter structure-level redundancy and finally learns a DNN to support batch querying.
- We built a prototype DEHYDRATOR and evaluated it on seven datasets totaling over one billion logs. Experimental results show that DEHYDRATOR reduces the storage space by 84.55%. DEHYDRATOR is  $7.36 \times$  more efficient than PostgreSQL,  $7.16 \times$  than Neo4j, and  $16.17 \times$  than Leonard. The code and data in this study will be open-sourced upon publication.
- We conducted a comprehensive evaluation of DEHYDRATOR, exploring the component impact, applicable scenario, and lower bound performance. Additionally, we defined the Latency-to-Storage Ratio, a metric that balances storage overhead and latency, and observed the impact of model capacity on this metric.

## II. BACKGROUND & INSIGHTS

### A. Provenance Graph

A typical endpoint detection and response (EDR) system captures streaming kernel logs by invoking an audit framework and represents the provenance graph with a node table and an edge table [38], [41], [42]. Specifically, a provenance graph  $G(E, V)$  is a heterogeneous directed graph consisting of nodes  $V$  representing system entities and edges  $E$  representing inter-entity interactions. The fields of nodes and edges are carefully selected from raw audit logs, which are lean and critical.

After observing several threat hunting and attack investigation systems [41], [43], [44], [18], [17], [19], [20], [21], [22], we found that the fields saved for nodes and edges can be categorized into three types: unique values (e.g., unique identifiers), incremental values (e.g., timestamps), and repetitive values (e.g., node types or event operations). Unique values can be replaced with shorter characters, incremental values with offsets, and repetitive values with indexes. These methods handling *field-level redundancy* are effective in reducing storage space [37], [39], [40], [38]. However, the storage

space for edge information is often significantly larger than the node. For example, when storing the provenance graph for the CADETS group of DARPA TC program [45], we need 42MB of space for the node table but 1,227MB for the edge table ( $\sim 29.21 \times$ ). This is because the operating system handles tasks through numerous system calls. In the provenance graph, this is represented by multiple parallel edges between node pairs, which we refer to as *structure-level redundancy*.

### B. Forensic Analysis

The goal of forensic analysis using provenance graphs [17], [22], [46], [13], [47], [48], [43], [49], [42] is to determine the source and scope of the attack, ascertain the extent of disruption, and develop remediation and prevention strategies. Typically, analysts perform backtracking from the Point of Interest (POI), iteratively searching for all dependencies related to the current event, similar to a state-constrained reverse breadth-first search (BFS). We also observe that the dependency explosion problem [38], [48], [50] causes the number of queries to increase exponentially with the number of iterations. For instance, in the DEPIMPACT dataset [48], obtaining a backtracking graph starting from the POI node (/tmp/leaked) requires over one million events. *We propose modeling the provenance graph as a directed hierarchical graph and performing hierarchical encoding of edges between different hierarchies.*

### C. DNN-based Storage System

A DNN model is a function capable of learning and representing complex patterns and features within data. Researchers model the storage task as a sequence generation task by building and training a DNN model to capture the data's characteristics and patterns, subsequently using the model to generate the sequence [33], [51]. During the storage phase, the DNN parameters are optimized on the target data using gradient descent algorithms to fit the data distribution, ultimately retaining only the DNN model while discarding the original data. During the query phase, given an input sequence (i.e., the query statement  $q$ ), the DNN can iteratively predict the next character and ultimately outputs a string  $s$  containing all information. Provenance graph storage is a typical *cold storage* task, where data is queried but not modified. Unlike traditional techniques [52], [53] attempt to balance storage efficiency with processing overhead, we focus instead on minimizing overall data size with query support. This emphasis makes time-consuming but storage-efficient DNN-based storage highly applicable. Furthermore, querying DNNs shows better performance than logic-based systems. DNNs inherently support batch queries (e.g., parallelism), which can effectively improve the infrastructure layer performance.

From Section II-A, we get **Key Insight I**: Achieving efficient and lossless storage requires handling both field-level redundancy and structure-level redundancy, with the latter being more critical. From Section II-B and II-C, we get **Key Insight II**: Hierarchical coding of edges reduces structure-level redundancy, accelerates model training, and supports reverse queries. **Key Insight III**: DNN-based storage

with specific structures and capacity can better fit encoded provenance graphs, thereby achieving storage-efficient and query-support.

## III. SYSTEM DESIGN

In this section, we will introduce the design details of each stage of DEHYDRATOR. As shown in Figure 1, DEHYDRATOR is a three-stage framework (i.e., pretreatment, storage, and query) to achieve efficient storage of provenance graphs and support the upper-layer components.

### A. Pretreatment

DEHYDRATOR leverages mature system auditing frameworks [54], [55], [56], [57] to collect raw logs about system calls from the kernel. Then DEHYDRATOR parses the collected raw logs to build a provenance graph, where nodes represent system entities and edges represent system events. Specifically, DEHYDRATOR carefully captures fields using regular expressions. The fields are lean and critical, as shown in Tables I. DEHYDRATOR logically views the unification of two tables (i.e., node table  $NT$  and edge table  $ET$ ) as a provenance graph  $G(V, E)$ , which is a common practice [41], [44], [48], [40]. FOR the node table  $NT$ , DEHYDRATOR preserves  $IdentID$  (the unique identifier for the node),  $Name$ , and  $Type$  (i.e., file/process/socket). FOR the edge table  $ET$ , DEHYDRATOR preserves  $SrcID$ ,  $DstID$ ,  $TimeStamp$  (Unix), and  $Operation$  (e.g., read/write/execute). Notably, the concatenation of  $SrcID$  and  $DstID$  is the  $IdentID$  because of the graph structure.

Based on **Key Insight I**, DEHYDRATOR then addresses three types of field-level redundancy (unique, repetitive, and incremental values) through **Field Mapping Encoding**. FOR unique and repetitive values, DEHYDRATOR replaces them with shorter numerical characters. FOR example, DEHYDRATOR uses the numeric character 0 to replace the frequently occurring string `Process` in the  $Type$  field of the node table  $NT$ . FOR incremental values, DEHYDRATOR obtains the minimum value and replaces them with offsets. FOR instance, if a timestamp is 1522706865 and the minimum value is 1522706824, DEHYDRATOR will replace 1522706865 with 41. Finally, DEHYDRATOR will retain three tables: an encoded node table  $NT_{en}$ , an encoded edge table  $ET_{en}$ , and a mapping table  $MT$ , as shown in Figure 1.

It should be noted that we have retained only the necessary fields to support upper-layer analysis components. However, in practice, DEHYDRATOR can modify regular expressions to augment the provenance graph's fields according to specific requirements, such as  $PID$  or  $HostID$ . DEHYDRATOR can automatically perform field-level redundancy filtering based on the type of newly added fields, demonstrating significant extensibility. In this paper, we exclusively utilize the fields presented in Table I.

### B. Storage

In this section, DEHYDRATOR achieves efficient storage of the encoded edge table  $ET_{en}$  through two steps: (1)

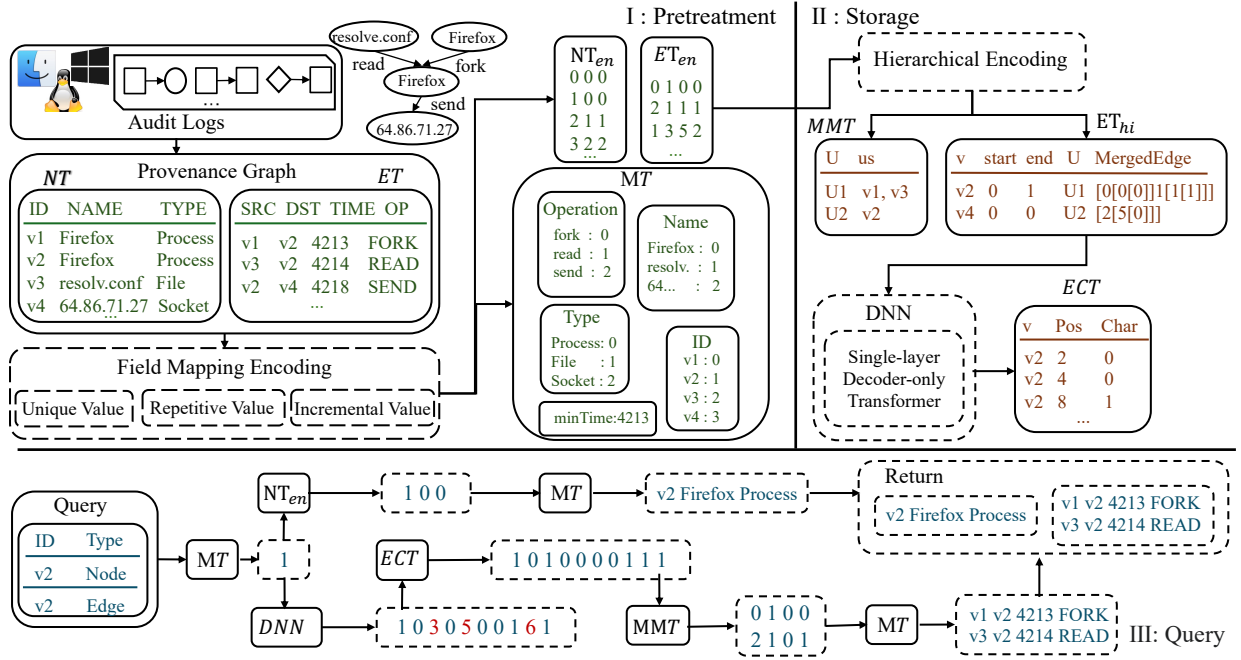


Fig. 1: Overview of DEHYDRATOR

TABLE I: Fields in node and edge tables and their corresponding examples and styles.

Table	Field	Example	Style
Node	IdentID	F487A907	Unique
	Name	Imapd	Repetitive
	Type	File/Process/Socket	Repetitive
Edge	SrcID	A603443D	Unique
	DstID	388D98ED	Unique
	TimeStamp	1522706865	Incremental
	Operation	Read/Write/Execute Sendto/Recvfr/FORK	Repetitive

Hierarchical Encoding, and (2) Model Training. The former is based on **Key Insight II** and filters structure-level redundancy. The latter is based on **Key Insight III** and supports batch queries.

1) *Hierarchical Encoding: Elucidation.* Firstly, we explain why applying hierarchical encoding to  $ET_{en}$  before model training. We model the provenance graph storage task as a sequence generation task, i.e., inputting a sequence and predicting the next character. Besides, we observe that while modern deep neural networks possess complex feature recognition and fitting capabilities, the manifestation of these capabilities requires larger parameter scales and training times. Pre-processed high-dimensional, dense input data can effectively mitigate this issue. This approach has been widely applied in natural language processing [58], [59]. For instance, when performing text generation tasks, words are first vectorized using word2vec [60] in the NLP domain. Therefore, we apply hierarchical encoding to increase the information density of input sequences, which significantly improves the training speed and model performance, as shown in Section IV-D.

Secondly, we explain why choosing hierarchical encoding. We observe that the direction of most upper-layer analysis components is reversed [17], [22], [46], [13], [47], [48], [43], [49], [42]. Specifically, when an EDR issues an alert, analysts typically perform multiple queries on the provenance graph

based on the infrastructure layer to investigate attack traces and impact scope (i.e., causality analysis), and this process is reversed. Besides, analysts usually use reverse information from the alert point to determine whether the alert is a false positive. We consider this process as a reverse breadth-first search of the provenance graph with conditional constraints. Based on this observation, we model the provenance graph as a directed hierarchical graph and encode different hierarchies separately (i.e., hierarchical encoding), thereby reducing structure-level redundancy.

**Procedure.** Here, we provide a detailed procedure for hierarchical encoding. In simple terms, *hierarchical encoding is a compact coding form that represents all incoming edges for each node*, an intuitive form of modeling provenance graph queries as reverse breadth-first searches. As shown in Figure 2, the specific process can be divided into two phases: **Traversal & Hierarchy** ( $A \rightarrow B$ ), and **Merging & Encoding** ( $B \rightarrow C$ ).

First, DEHYDRATOR traverses the provenance graph, recording all source nodes and incoming edges for each node  $v$ , as shown in Lines 6 to 8 of Algorithm 1. DEHYDRATOR treats each node  $v$  and its incoming edges as a hierarchical subgraph, represented by the gray boxes in part B of Figure 2. Then, DEHYDRATOR save the mapping of all nodes to their source nodes into the  $MMT$  and all incoming edges into  $MergedEdge$ , as shown in Lines 10 to 15 of Algorithm 1. Next, DEHYDRATOR saves the minimum and maximum timestamps from all incoming edges as  $startTime$  and  $endTime$ , as demonstrated in Lines 16 and 17. Finally, DEHYDRATOR stores the encoded data into hierarchical edge table  $ET_{hi}$  in the format  $[v, startTime, endTime, U_v, MergedEdge]$  as shown in Line 18. DEHYDRATOR places  $v$  at the beginning to serve as a header, supporting the query requirement of DNN-based storage systems.  $startTime$  and  $endTime$  immediately follow because we observe that temporal constraints are the most common in provenance graph queries by upper-layer

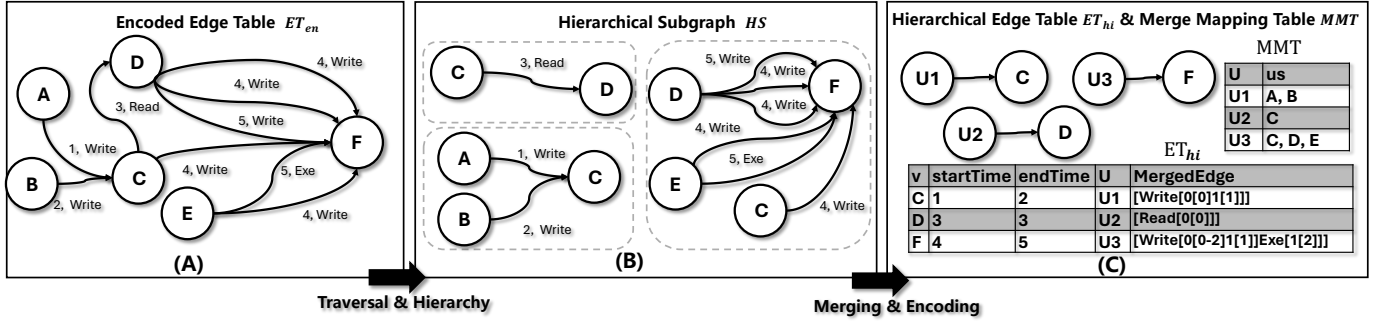


Fig. 2: Hierarchical Encoding.

analysis components.

The function *MergeEdges* combines all edges into a nested list *MergedEdge*, as shown in Part C of Figure 2. The structure of the nested list is: **[Operation: [timeOffset: [nodeOffset]]]**, where  $timeOffset = e.timestamp - startTime$ ,  $nodeOffset = e.v.Location$  in  $U_v$ . We designed the list's nesting order based on the amount of redundancy. Firstly, we observed that given a node  $v$ , the most frequently repeated field among all its incoming edges is **Operation**. For example, For  $\forall e \in E$  where  $e.dstID.type = File \rightarrow e.Operation \in (Write, Exe)$ . The second most repeated field is **timeOffset**. Due to the complexity and efficiency of modern operating systems, a process node may have hundreds of simultaneously generated incoming edges during initialization. As for **nodeOffset**, we represent long incremental sequences using shorter format. For example, [1,2,3,5,7,8,9] is represented as [1-3,5,7-9].

Finally, DEHYDRATOR preserves  $MMT$  and  $ET_{hi}$ , which denotes dense information of all incoming edges  $E_v$  of each node  $v$  for model training. The effectiveness of hierarchical encoding is influenced by the graph structure, a situation we discuss thoroughly in Section IV-D and Section IV-E.

2) *Model Training*: As described in Section II-C, we model the storage task as a sequence generation task. Specifically, DEHYDRATOR functions as a database-like storage system: when a user inputs a query statement  $q$ , the DNN outputs a return string  $s$  containing all relevant information. Besides, we learn a DNN to support batch queries.

**Model Selection.** The DNN's output is achieved through iterative input of the generated sequence, i.e., an autoregressive model [61], [62], [63] (e.g., LSTM [64], GRU [65], Transformer [59]). LSTM and GRU build long-term dependency based on a sequential process, where each hidden state needs to wait for output from previous steps. Transformers build history dependency parallel, which has a better chance of fully utilizing GPU. Standard transformers have deep and heavy model structures whose parameters often reach 300M [66], [67], [68]. This is because the transformer was originally designed to process linguistic knowledge, requiring the ability to extract high-level semantic features from text. Storage, although modeled as a sequence generation task, focuses more on detecting low-level and repetitive patterns. We believe a single transformer layer is powerful enough to adapt to storage tasks. Furthermore, encoder-only transformers are simpler, have fewer training parameters, and inherently align with

### Algorithm 1 Hierarchical Encoding Algorithm

#### Require:

- 1: (1) Encoded Edge Table  $ET_{en}$ ;
- 2: (2) Hierarchical Edge Table  $ET_{hi}$ ;
- 3: (3) Merge Mapping Table  $MMT$ ;
- 4: (4) An Empty Dict  $Dict$  and two Empty Lists  $U_v$  &  $E_v$ ;
- 5: (5) Func for Merging Edge Information *MergeEdges*;
- 6: **for**  $e = (u, v, timestamp, operation) \in ET_{en}$  **do**
- 7:      $Dict[v].append(u)$ ;
- 8:      $Dict[(u, v)].append(e)$
- 9: **end for**
- 10: **for**  $v \in Dict.keys()$  **do**
- 11:     **for**  $u \in Dict[v]$  **do**
- 12:          $MMT[U_v].append(u)$
- 13:          $E_v.append(Dict[(u, v)])$
- 14:     **end for**
- 15:      $MergedEdge = MergeEdges(E_v)$
- 16:      $startTime = \min([e.timestamp \text{ for } e \text{ in } Dict[(u, v)])]$
- 17:      $endTime = \max([e.timestamp \text{ for } e \text{ in } Dict[(u, v)])]$
- 18:      $ET_{hi}.append([v, startTime, endTime, U_v,$
- 19:          $MergedEdge])$
- 20:      $U_v \leftarrow \emptyset, E_v \leftarrow \emptyset$
- 21: **end for**
- 22:
- 23: **return**  $ET_{hi}$

sequence generation tasks [69], [62]. Consequently, we opted for a single-layer, decoder-only transformer. This opinion is validated in the experiment section.

**Training & Error Correction.** Initially, DEHYDRATOR converts each edge in  $ET_{hi}$  into a string " $v, startTime, endTime, U_v, MergedEdge$ ", where  $v$  represents the target node and serves as the query head,  $U_v$  denotes the index of merged source nodes, and *MergedEdge* represents the merged edge information of incoming edges. Subsequently, DEHYDRATOR directly employs the `char2vec` method [70] to encode the string into numerical vectors. DEHYDRATOR then automatically identifies the minimum length  $L$  from the query head to the terminator across all strings, and uses this to segment all data. Finally, DEHYDRATOR inputs all segmented data into the model for training and terminates the process after reaching the

maximum epoch or model fitting.

We model the storage task as a sequence generation task; however, training a zero-error model for a content-rich file is challenging. This conflicts with the need for **Content-lossless** proposed in Section I. To address this issue, we employ an Error Correction Table (*ECT*). Specifically, we first test the trained model by sequentially inputting  $v$  and comparing the model's final output with the dataset. If inconsistent, we record ( $v : [p : c]$ ) in the *ECT*, where  $v$  represents the query head,  $p$  indicates the error position and  $c$  denotes the correct character. Finally, we preserve this *ECT* to correct the model's generated content when supporting query requirements of upper-layer analysis components. This mechanism is similar to existing work [40].

### C. Query

DEHYDRATOR, as an efficient infrastructure layer, supports query requirements of upper-layer analysis components. We describe the process in the context of Figure 1. FOR node information, given a node's *IdentiID* **v2**, DEHYDRATOR obtains its index value **1** via *MT* mapping ( $IndexValue = MT(IdentiID)$ ). Then DEHYDRATOR searches in the encoded node table  $NT_{en}$  by index, and retrieves node information (**v2 Firefox Process**) through *MT* inverse mapping ( $Information = MT\_REVERSE(NT_{en}(IndexValue))$ ). FOR edge information, DEHYDRATOR inputs the index value into the model, generating the corresponding sequence [**1 0 3 0 5 0 0 1 6 1**] through autoregression ( $Seq = DNN(IndexValue)$ ). Subsequently, DEHYDRATOR employs *ECT* for error correction, obtaining a fully accurate sequence [**1 0 1 0 0 0 0 1 1 1**] ( $AccSeq = ECT(Seq)$ ). Finally, DEHYDRATOR performs hierarchical decoding and *MT* inverse mapping on the generated sequence to retrieve readable information [**v1 v2 4213 FORK**], [**v3 v2 4214 READ**] for all incoming edges ( $Information = MT\_REVERSE(HierDecode(AccSeq))$ ).

## IV. EVALUATION

In this section, we first introduce the experimental protocol, including the environment, baselines, metrics, datasets, and hyperparameters. Subsequently, we provide a detailed assessment of the costs with storage and query of provenance graphs. Then, we demonstrate the significance of each component of DEHYDRATOR. Furthermore, we determine the applicable scenario and lower bound performance of DEHYDRATOR. Finally, we explore the impact of model selection and capacity on DEHYDRATOR. In summary, we aim to answer the following questions:

- **RQ1:** What is the performance of DEHYDRATOR on provenance graph storage?
- **RQ2:** How efficient is DEHYDRATOR in supporting provenance graph queries?
- **RQ3:** How important is each component of DEHYDRATOR?
- **RQ4:** What is the applicable scenario and lower bound performance of DEHYDRATOR?
- **RQ5:** What is the impact of model selection and capacity on DEHYDRATOR?

### A. Experimental Protocol

**Environment.** DEHYDRATOR is implemented using Python 3.9 with PyTorch 1.13.1 and scikit-learn 1.2.0, used for training DNN models, respectively. Our experiments are all carried out on a server running Ubuntu 20.04 64-bit OS with AMD EPYC 7513 32-Core Processor, 256GB memory, and RTX A6000 GPU.

**Baselines.** We have selected existing state-of-the-art systems as baselines for comparison with DEHYDRATOR: PostgreSQL [71] (a relational database), Neo4j [34] (a graph database), and LEONARD [40] (a DNN-based storage system).

**Metrics.** We define the storage overhead (bytes) of the pre-processed provenance graph as  $BP_{pre}$ , the post-processed as  $BP_{post}$ , and the storage latency as  $T_s$ . Specifically,  $BP_{pre}$  represents the bytes of the *ET*, while  $BP_{post}$  is the bytes for three files (*MMT*, *DNN*, and *ECT*). Considering that *ET* occupies more than 95% of the space in the provenance graph, we prefer to evaluate the efficiency of DEHYDRATOR in storing *ET*, thus equating  $BP_{pre}$  to *ET*. The Latency-to-Storage Ratio (LSR) is defined as  $LSR = (BP_{pre} - BP_{post})/T_s$ .

**Datasets.** We evaluate DEHYDRATOR on a dataset containing over one billion raw logs. As shown in Table II, this dataset comprises seven provenance graphs (G1-G7). G1-G4 are sourced from the CADETS (G1), THEIA (G2), and TRACE (G3, G4) groups of DARPA TC E3 [45], G5-G6 are from the TRACE group of DARPA TC E4, G7 is a subset of the DEPIMACT dataset [48]. G1-G6 were collected using SPADE [72], while G7 is collected using Sysdig [73]. The second column, "Log Size," indicates the size of the raw log files collected by the capture layer [72], [73], i.e., JSON files. The third column, "Graph Size," represents the size of the provenance graphs, i.e.,  $BP_{pre}$ . The fourth column, "# Nodes," and the fifth column, "# Edges," denote the number of nodes and edges in the provenance graph. *Regarding the average edges of provenance graphs ( $\sim 17,754,566$ ), we are 9.6  $\times$  larger than Leonard ( $\sim 1,849,833$ ).*

**Hyperparameters.** Unless otherwise specified, DEHYDRATOR uses the same hyperparameters. Specifically, DEHYDRATOR employs the Single-layer Decoder-only Transformer model described in Section III-B2. The default training settings for the dataset are batch size 4,096, Adam optimizer, learning rate 0.001, and maximal training epoch 5, with an early stopping mechanism. Additionally, the length of segments for different provenance graphs in the dataset is adaptive and different. Finally, we design several models with different capacities (i.e., embedding dimension, number of attentional heads, and feedforward dimension) to evaluate the impact of model capacity on DEHYDRATOR, as shown in Table III.

### B. Storing Provenance Graphs

To address RQ1, we evaluate the storage overhead and latency of DEHYDRATOR and different baselines (PostgreSQL, Neo4j, and Leonard) operating on various datasets with metrics  $BP_{post}$ ,  $T_s$ . For PostgreSQL, we use the built-in COPY command to store the provenance graphs from CSV files [74]. For Neo4j, we utilize the *neo4j-admin import* tool to store the

TABLE II: Overview of Datasets

Label	Log Size (GB)	Graph Size (MB)	# Nodes	# Edges
G1	38.34	1226.72	414,518	13,244,643
G2	85.19	2750.08	1,144,475	29,655,652
G3	25.56	712.92	812,083	7,628,155
G4	26.89	713.84	816,730	7,717,378
G5	32.05	1152.30	1,001,005	12,536,153
G6	33.06	1164.28	966,490	12,691,262
G7	31.89	3470.72	432,379	40,808,719
<b>Avg</b>	<b>38.99</b>	<b>1598.69</b>	<b>798,240</b>	<b>17,754,566</b>

TABLE III: Models with Different Capacities. Column 1 is the capacity (M is short for MEGABYTE) of the models. Columns 2 through 4 are adjustable hyperparameters. Column 5 is the number of parameters.

Capacity (M)	Embedding Dimension	Attention Head	Feedforward Dimension	Parameters (K)
C1 (0.08)	32	1	128	18
C2 (0.28)	64	2	256	70
C3 (1.1)	128	4	512	271
C4 (2.4)	192	6	768	600
C5 (4.1)	256	8	1,024	1,070
C6 (9.2)	384	12	1,536	2,380

provenance graphs [75], specializing in storing large graphs. For Leonard<sup>1</sup>, we modify the parsing component to take the *ET* as input while keeping other components unchanged. We also increase  $\#Parameters$  of the multilayer LSTM to 64K to align ours. We email the authors and will also open-source this modified version of Leonard upon publication.

Table IV shows the storage overhead and latency of different techniques for storing provenance graphs. As can be observed, the average storage overhead for the relational database PostgreSQL is 1,818M, while for the graph database Neo4j it is 1,770M, both slightly larger than the original provenance graphs ( $\sim 1,598M$ ). These traditional databases build indices and maintain metadata to enhance query performance when storing data. Leonard performs the worst, with an average storage overhead of 3,991M, which is  $2.5 \times$  larger than the original provenance graphs. Leonard fails to achieve efficient storage of provenance graphs, strikingly different from the performance reported in the original paper [40]. DEHYDRATOR demonstrates the best storage performance, at only 247M, which is  $7.36 \times$  smaller than PostgreSQL,  $7.16 \times$  smaller than Neo4j, and  $16.17 \times$  smaller than Leonard.

DEHYDRATOR significantly outperforms Leonard, and there are four reasons for this. (1) Evaluation Metric. Leonard evaluates storage overhead on the gzip-compressed *ECT* file, where a 3592M *ECT* is compressed to a 68M gz file. However, the storage system needs to decompress this gz file and load it into memory to support queries, which requires significant time (138s) and memory overhead (3.6G). We therefore use the size of raw *ECT* (JSON File) as an evaluation metric for storage overhead. (2) Dataset Complexity. The average number of edges and degrees in our dataset ( $\sim 17,754,566$ ,  $\sim 22.24$ ) are  $9.6 \times$  and  $11.7 \times$  those of Leonard ( $\sim 1,849,833$ ,  $\sim 1.89$ ) respectively. In non-Euclidean space, the complexity of the graph structure may exceed Leonard’s processing boundaries. Furthermore, we only involve 4 fields (SrcID, dstID, Operation, and Timestamp), while Leonard

has 13. We believe that Leonard’s reported efficient storage capability stems mainly from filtering field-level redundancy but ignoring structure-level redundancy. (3) Hierarchical Encoding. We can view hierarchical encoding as an operation that aggregates information to increase data density. This heuristic approach helps the model avoid learning patterns directly from low-dimensional redundant underlying data, thereby improving the speed and effectiveness of model fitting [58], [59]. Leonard trains the model directly on the raw data, resulting in a large *ECT* due to the inability to fit (loss hovers around 2). Section IV-D also demonstrates the impact of hierarchical encoding on training speed and model performance. (4) Model Capability. Leonard uses multi-layer LSTM, while we chose a Single-layer Decoder-only Transformer. With the same number of parameters, the latter can better learn complex patterns and interactions among high-dimensional data processed by hierarchical encoding. Its powerful representational ability and efficient attention mechanism allow the model to fit with only a few epochs of training (generally within 4 epochs) [59], [76], [77].

In terms of storage latency, Neo4j is the fastest with an average time of 21 seconds, followed by PostgreSQL with an average time of 45 seconds. Leonard performs the worst, with an average latency of 30,233 seconds, while DEHYDRATOR is 3,205 seconds. The low efficiency of existing model training and inference frameworks causes high time costs. Adopting advanced technology and using powerful machines can decrease costs. According to statistics, the average period of these datasets is 6.7 hours, and DEHYDRATOR’s storage latency accounts for 13.29% of that period. Considering cold storage scenarios, the storage latency of DEHYDRATOR is acceptable.

Furthermore, we observe that the storage overhead and time costs of DEHYDRATOR don’t increase linearly with the size of the original provenance graph. For example, the size of G7’s provenance graph ( $\sim 3470M$ ) is  $2.98 \times$  of G5 ( $\sim 1152M$ ), but G7’s  $ET_{hi}$ ,  $MMT$ ,  $ECT$ , and  $T_s$  are 49.3M, 9.8M, 131M and 2,293s respectively, which are only 38% ( $\sim 128.6M$ ), 30% ( $\sim 33.1M$ ), 38% ( $\sim 345M$ ), and 53% ( $\sim 4335s$ ) of G5’s. We provide a detailed analysis of this phenomenon in Section IV-E. Finally, we also observe that model capacity affects the performance of DEHYDRATOR. We provide a detailed analysis of this in Section IV-F.

### C. Querying Provenance Grpahs

To evaluate the costs of querying with DEHYDRATOR, we measured the time cost of performing queries with DEHYDRATOR and compared the results with other systems. Different configurations can affect querying efficiency, and we evaluate the query cost using the smallest model (C2 in Table III) on Dataset G1, which is a common practice [37], [40], [50]. First, we randomly select 100 nodes from the provenance graph as query starting nodes. Then, we perform multiple BFSs (breadth-first searches) for each node. We refer to the number of BFS executions as the **Depth**. Many existing works [38], [48], [78], [42], [46], [79], given a POI (Point-of-Interest), first construct a backtracking provenance graph,

<sup>1</sup><https://github.com/dhl123/Leonard>



TABLE IV: Storage Overhead and Latency of Storing Provenance Graphs for Different Systems.  $BP_{post}$  and  $T_s$  denote the disk usage and latency of storing the provenance graph.  $MT$ ,  $DNN$ , and  $ECT$  represent the storage overhead for the merge mapping table, model, and error correction table. HE, Train, and Correct represent the time overhead for hierarchical encoding, model training, and error correction.

Dataset	PostgreSQL		Neo4j		Leonard				Dehydrator					
	$BP_{post}$ (MB)	$T_s$ (s)	$BP_{post}$ (MB)	$T_s$ (s)	$BP_{post}$ (MB)		$T_s$ (s)		$BP_{post}$ (MB)			$T_s$ (s)		
					$DNN$	$ECT$	Train	Correct	$MMT$	$DNN$	$ECT$	HE	Train	Correct
G1	1,362	33	1,367	17	0.9	3,592	15,273	7,628	8.8	1.1	51	55	660	429
G2	3,034	76	2,767	28	0.9	5,896	38,054	16,324	21.2	1.1	135	130	1,763	1,056
G3	786	20	1,037	15	0.9	2,217	8,913	4,517	26.8	1.1	252	79	2,709	1,724
G4	790	21	1,039	17	0.9	2,419	11,295	5,824	30.4	0.1	292	91	1,269	2,070
G5	1,287	32	1,306	19	0.9	3,659	14,078	7,058	33.1	1.1	345	111	1,924	2,300
G6	1,291	33	1,319	21	0.9	3,176	12,942	6,091	28.3	2.4	359	102	1,913	1,888
G7	4,177	103	3,556	33	0.9	7,001	43,206	20,433	9.8	1.1	131	166	879	1,122
<b>Avg</b>	<b>1,818</b>	<b>45</b>	<b>1,770</b>	<b>21</b>	<b>3,991</b>		<b>30,233</b>		<b>247</b>			<b>3,205</b>		

TABLE V: Time Costs of Querying at Different Depths for Different Systems.

Depth	D1				D2				D3				D4			
Quartile	Q1	Q2	Q3	Q4	Q1	Q2	Q3	Q4	Q1	Q2	Q3	Q4	Q1	Q2	Q3	Q4
Min	0	1	2	3	0	1	7	15	0	1	13	285	0	1	24	2300
Max	0	1	3	11	0	7	14	1571	0	13	285	17768	0	24	1440	48998
Mean	0	1	2	7	0	4	11	157	0	5	77	2127	0	6	356	17588
PostgreSQL (s)	0.45	0.45	0.45	0.44	0.42	1.65	1.72	1.62	0.43	1.82	2.98	3.59	0.44	1.97	4.55	486.60
Neo4j (s)	0.11	0.11	0.11	0.11	0.10	0.42	0.42	0.65	0.10	0.58	1.97	2.39	0.10	0.59	3.78	67.22
Dehydrator (s)	0.01	0.31	0.30	0.31	0.01	0.37	0.61	6.17	0.01	0.22	2.13	99.29	0.01	3.28	4.67	394.68

and this construction is a process involving multiple BFSs with time conditions. Therefore, we choose to execute the BFS algorithm on different nodes at different times to evaluate the query effectiveness of DEHYDRATOR.

Table V shows the time costs of querying at different depths for different systems. The first row, Depth, indicates the number of BFS executions, where we choose 1-4 (i.e., D1-D4). The second row, Quartile, represents the quartiles obtained by sorting nodes in ascending order based on the number of returned edges at that depth. For example, Q4 represents the set of nodes in the top 25% in terms of the number of returned edges. Rows 3-5, Min/Max/Mean, show the minimum, maximum, and average values of the edges returned by the nodes in the different quartiles. Rows 6-8 represent the query times at different depths for different systems. Leonard takes several minutes to load the huge  $ECT$ , so we don't compare querying cost with it.

As shown in Table V, Neo4j demonstrates the best overall performance ( $\sim 4.92s$ ), followed by DEHYDRATOR ( $\sim 32.02s$ ), with PostgreSQL performing the worst ( $\sim 32.08s$ ). Neo4j uses adjacency lists to store nodes and edges, making access to a node's incoming edges a fast, direct operation. On the other hand, PostgreSQL needs to scan row by row, while DEHYDRATOR needs to generate characters one by one, resulting in query efficiencies far inferior to Neo4j for both systems. We also attempted the case where Depth=5, but DEHYDRATOR required over 600s of generation time for most nodes, while PostgreSQL was unable to return results at all. Therefore, we did not include this in the table. PostgreSQL requires a significant amount of memory to store intermediate results, and when the depth is large, it encounters out-of-memory errors. DEHYDRATOR, however, does not face this issue. *On queries, DEHYDRATOR has similar efficiency to PostgreSQL.* Besides, the main reason for DEHYDRATOR's high latency is the inefficiency of existing model inference frameworks. The total query time consists of model inference time and

decoding time, with model inference time accounting for over 99% of the total. Given a query head, DEHYDRATOR constructs the  $Seq$  in the form of autoregressive generation, i.e., generating each character step by step. When the length of  $Seq$  corresponding to a node is large (for example, thousands), the autoregressive generation can cause high latency [59], [62], [63], [61]. Adopting advanced technologies and using more powerful machines can reduce this time cost.

In fact, DEHYDRATOR utilizes hierarchical encoding to enhance model inference speed like some works [80]. As discussed in Section III-B1, hierarchical encoding is a process that increases information density, meaning that the same information is represented with fewer characters. Hierarchical encoding can reduce the number of characters that need to be generated, decreasing the number of model inferences and reducing query latency.

#### D. Effect of Components

DEHYDRATOR performs field mapping encoding (FME) on the original provenance graph to obtain  $ET_{en}$ , then applies hierarchical encoding (HE) on  $ET_{en}$  to obtain  $ET_{hi}$  and  $MMT$ . Finally, it inputs  $ET_{hi}$  for the training model (TM) and error correction (EC) to obtain  $BP_{post}(ECT + DNN + MMT)$ .

First, we evaluate the effect on storage overhead of three components applied in DEHYDRATOR: field mapping encoding, hierarchical encoding, and model training. Specifically, we include the original size and the sizes of storing the same provenance graph after sequentially executing field mapping encoding, hierarchical encoding, and model training. For better viewing, we choose only five datasets here, namely G1, G2, G3, G5, and G7. The results are shown in Figure 3.

Figure 3(a) shows the storage overhead for storing graphs. The average size of  $ET_{en}$  is 405.2MB, which is 25.3% of the original provenance graph ( $\sim 1598.69MB$ ). The average size of  $ET_{hi}$  ( $\sim 75.98MB$ ) is 18.7% of  $ET_{en}$  and 4.7% of the original graph. There exists a large amount of field-level and



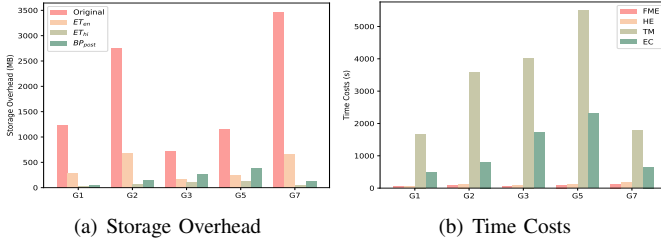


Fig. 3: Storage Overhead and time costs of Individual Components.

structure-level redundancy in the original provenance graph, thus both encodings achieve good compression results. After adding model training, the average storage overhead of DEHYDRATOR increases to 192.42MB, which is 12% of the original provenance graph. Increasing the number of model parameters and training epochs could reduce the final storage overhead, but the resulting latency would be intolerable, which will be discussed in detail in Section IV-F. Therefore, DEHYDRATOR uses model training not to further compression, but to provide a batch querying capability. Figure 3(b) shows the time costs for storing graphs. The average time costs for FME, HE, TN, and EC are 82.8s, 108.2s, 3307.8s, and 1195.6s respectively. FME and HE do not involve training, thus they are speedy. The combination of TN and EC is the model training component of DEHYDRATOR, as described in Section III-B2.

Then, we evaluate the impact of the hierarchical encoding component on model training. Specifically, we construct Dehydrator-wtHE, a version of Dehydrator without the hierarchical encoding. Intuitively, Dehydrator-wtHE directly applies the `char2vec` method [70] to encode the strings  $ET_{en}$  into numerical values  $ET_{hi}$ , which are then input into the model for training. Both Dehydrator and Dehydrator-wtHE use the same model (C2) on dataset G1 for the comparison experiment. Table VI shows the results. Firstly, the  $ET_{hi}$  size and number of segments for Dehydrator (20.19M, 21,169,175) are only 7.5% of those for Dehydrator-wtHE (268.31M, 281,340,212). This is because HE reduces structure-level redundancy, resulting in the former's model training time (660.69s) being  $8.8 \times$  smaller than the latter (5814.42s). Furthermore, due to the low information density in Dehydrator-wtHE's  $ET_{hi}$ , the model is unable to fit properly, resulting in a high Loss value of 1.58. Finally, the Dehydrator's EC time (429.51s) and  $ECT$  size (50.79M) are  $19.48 \times$  and  $20.95 \times$  smaller than those of Dehydrator-wtHE (8370.52s, 1064.25M), respectively. *Therefore, we believe that the hierarchical encoding component can significantly improve the training speed and model performance.*

### E. Applicable Scenario & Lower Bound

As described in Section IV-D, field mapping encoding and hierarchical encoding are both effective in removing redundancy. However, the former applies to arbitrarily structured provenance graphs, while the latter does not. Therefore, we provide the applicable scenario for hierarchical encoding.

The hierarchical encoding stage focuses on reducing structure-level redundancy, with  $ET_{en}$  as input and  $ET_{hi}$  as

TABLE VI: Impact of Hierarchical Encoding on Model Training. Row 2 indicates the size of  $ET_{hi}$ , Rows 3 and 4 indicate the number and length of segments, Rows 5 and 6 indicate the model training time and final loss. Rows 7 and 8 indicate the error correction time and the size of  $ECT$ .

Systems	Dehydrator	Dehydrator-wtHE
$ET_{hi}$ (M)	20.19	268.31
Segment Num	21,169,175	281,340,212
Segment Length	23	8
Train (s)	660.69	5,814.42
Final Loss	0.88	1.58
EC (s)	429.51	8,370.52
ECT (M)	50.79	1,064.25

output. In a provenance graph  $G = (V, E)$ , the number of nodes is denoted by  $n = |V|$ , the number of edges is denoted by  $m = |E|$ , and the average degree is  $d_{avg} = \frac{m}{n}$ . Furthermore, we define the space occupation in bytes for each field -  $srcID$ ,  $dstID$ ,  $timestamp$ , and  $operation$  - as  $BS_s$ ,  $BS_d$ ,  $BS_t$ , and  $BS_o$  respectively. Thus, the byte size of  $ET_{en}$  is denoted as:

$$BS_{ET_{en}} = m * (BS_s + BS_d + BS_t + BS_o) \quad (1)$$

For node  $v \in V$ , let its number of parent nodes be  $p_v$ , and its number of incoming edges be  $m_v$ . After hierarchical encoding, the edge is structured as  $e_{hi} = [v, U_v, startTime, endTime, MergedEdge_v]$ , where  $MergedEdge_v = [Operation[timeOffset[nodeOffset]]]$ . Among these, the byte sizes of  $v$ ,  $startTime$ ,  $endTime$ , and  $U$  are  $BS_d$ ,  $BS_t$ ,  $BS_t$ , and  $p_v * BS_s$ , respectively. To calculate the byte size of the content  $BS_{con_v}$ , we assume the number of retained unique entries in the  $Operation$  field after deduplication is  $m_{vo}$ , the number of retained unique entries in the  $timeOffset$  field under each  $Operation$  after deduplication is  $m_{vot}$ , and the number of retained unique entries in the  $nodeOffset$  field under each  $timeOffset$  after deduplication is  $m_{votn}$ . Then the byte size of  $MergedEdge_v$  is:

$$BS_{con_v} = BS_o * m_{vo} + BS_t * \sum_{O_v}^o * m_{vot} + BS_s * \sum_{O_v}^p \sum_{T_v}^t * m_{votn} \quad (2)$$

where  $\sum_{O_v}^o \sum_{T_v}^t * m_{votn} = m_v$ . Therefore, the byte size of  $ET_{hi}$  is:

$$BS_{ET_{hi}} = \sum_V^v (BS_o * m_{vo} + BS_t * (\sum_{O_v}^o * m_{vot} + 2) + BS_s * (p_v + m_v) + BS_d) \quad (3)$$

In Section III-A, we performed index mapping for different fields, so these fields are all fixed and equal in size (int4 type, 32 bits). Therefore, we can abbreviate both as:

$$BS_{ET_{en}} = 4 * m$$

$$BS_{ET_{hi}} = \sum_V^v m_{vo} + \sum_V^v \sum_{O_v}^o m_{vot} + \sum_V^v p_v + 3n + m \quad (4)$$

Considering that  $\sum_V^v m_{vo} \leq 3n$  (a node can have at most 3 operations of incoming edges, for example, a process node can have operations of Read, Sendto, and Fork),  $\sum_V^v \sum_{O_v}^o m_{vot} \leq m$  and  $\sum_V^v p_v \leq m$ , therefore:

$$BS_{ET_{en}} - BS_{ET_{hi}} \geq 0, \text{ If } \frac{m}{n} \geq 3 \quad (5)$$

where  $d_{avg} = \frac{m}{n}$ . Therefore, for hierarchical encoding, as long

TABLE VII: The Impact of Degree on Hierarchical Encoding.

Dataset	P1	P2	P3	P4	P5
$BP_{pre}$ (M)			304.89		
# Edge			5,000,000		
$ET_{en}$ (M)			96.46		
Degree	1	2	3	4	5
$ET_{hi}$ (M)	171.67	102.12	78.31	66.35	59.16
Applicable	No	No	Yes	Yes	Yes

as the degree  $d_{avg} \geq 3$ , it constitutes an effective encoding scenario, capable of filtering structure-level redundancy and enhancing information density. Due to the high concurrency and complexity of modern operating systems, provenance graphs often have degree values far exceeding this threshold, as shown in Section IV-A.

We also conduct experiments to prove the above conclusion. Specifically, we generated 5 datasets in a laboratory environment, each consisting of 5 million events, with average degrees of 1, 2, 3, 4, and 5, respectively, referred to as P1-P5. We consider that  $ET_{hi} < ET_{en}$  indicates that hierarchical encoding is effective. As shown in Table VII, hierarchical encoding is demonstrated to apply to the three datasets P3, P4, and P5. This proves that hierarchical encoding effectively filters structure-level redundancy on provenance graphs with  $d_{avg} \geq 3$ , as shown in our derivation above.

The applicable scenario of DEHYDRATOR is for provenance graphs with  $d_{avg} \geq 3$ . When the  $d_{avg} = 1$ , DEHYDRATOR exhibits a lower bound performance.

#### F. Model Selection and Capacity

We consider model training as a form of utilizing the memory and batch querying capabilities of DNN models to encode provenance graphs. In this section we evaluate the impact of model selection and capacity on DEHYDRATOR respectively.

**Model Selection.** As mentioned in Section III-B2, we chose the Single-layer Decoder-only Transformer (SDT) as our base model and compared it with two other models: Multi-Layer LSTM and Multi-Layer GRU. To ensure fairness, all three are compared in G1 and have similar parameter counts. Specifically, SDT has 70K parameters (C2), LSTM has 64K (Embedding Dimension=32, Hidden Dimension=64, Layer=2), and GRU has 74K (Embedding Dimension=32, Hidden Dimension=64, Layer=3). As shown in Table VIII, SDT's training time ( $\sim 660s$ ) is  $1.29 \times$  that of LSTM ( $\sim 510s$ ) and  $1.21 \times$  that of GRU ( $\sim 544s$ ). The generated ECT ( $\sim 50.79M$ ) is 66.50% of LSTM ( $\sim 76.38M$ ) and 73.55% of GRU ( $\sim 69.05M$ ). The purpose of DEHYDRATOR is to efficiently store provenance graphs. SDT has stronger feature extraction and pattern recognition capabilities, allowing it to better fit the high-density information in  $ET_{hi}$ , resulting in a smaller  $ECT$ . Therefore, we choose the Single-layer Decoder-only Transformer as the base model for DEHYDRATOR.

**Model Capacity.** Existing research has already demonstrated that the 'double descent curve' is a robust phenomenon in modern neural networks, indicating that 'larger models are better' [81], [82], [83]. However, storage scenarios must balance latency and effectiveness. For instance, if the storage latency exceeds the period of the provenance graph, such

TABLE VIII: Impact of Model Selection on model training and error correction.

Model Selection	Single-layer Decode-only Transformer	Multi-layer LSTM	Multi-layer GRU
Train (s)	660	<b>510</b>	544
Final Loss	<b>0.88</b>	1.12	1.00
EC (s)	429	<b>397</b>	408
ECT (M)	<b>50.79</b>	76.38	69.05

storage becomes akin to chasing a carrot. Therefore, we designed a simple yet effective metric called *Latency-to-Storage Ratio (LSR)* to evaluate the efficiency of the model training. Assuming the time cost of the storing is  $T_s$ , the byte size of pre-processing logs is  $BS_{pre}$ , and the byte size of post-processing logs is  $BS_{post}$ ,  $LSR$  is defined as:

$$LSR = \frac{BS_{pre} - BS_{post}}{T} (B/s) \quad (6)$$

where  $B/s$  denotes the average number of bytes compressed per second.

Given a provenance graph  $G$ , we observe that the model capacity  $MC$  is a key variable that affects both storage overhead and latency. We construct 6 different capacities of models, as shown in Table III, and conduct evaluation experiments on datasets, recording  $BS_{pre} - BS_{post}$ ,  $T_s$ , and  $LSR$ . Figure 4 shows the result. As shown in Figure 4(a) and Figure 4(b), when the  $MC$  increases, both storage overhead  $BS_{pre} - BS_{post}$  and latency  $T_s$  rise, with the latter increasing at a faster rate. As depicted in Figure 4(c) and Figure 4(d), the curve in the graph resembles a skewed distribution, i.e., there exists a value  $\eta$  such that when  $MC = \eta$ ,  $LSR$  reaches its maximum. For G4,  $\eta = C1$ , for G6,  $\eta = C3$ , for other provenance graphs,  $\eta = C2$ . *Larger model is not always better, and different provenance graphs have different  $\eta$ .* Like most storage systems, DEHYDRATOR also needs to balance storage overhead and latency. If higher storage efficiency is prioritized, a model with larger capacity is used. If lower latency is prioritized, a model with smaller capacity is used.

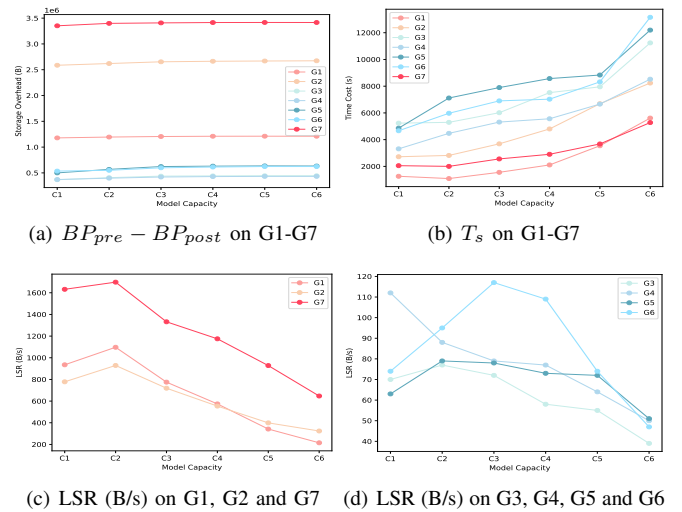


Fig. 4: Impact of Model Capacity.

## V. DISCUSSION

The purpose of DEHYDRATOR is to store provenance graphs efficiently. DEHYDRATOR saves  $MMT$ ,  $DNN$ , and  $ECT$  to

enable event querying on the provenance graph, with *ECT* accounting for over 90% of the space. Naturally, we try to minimize *ECT* as much as possible to further reduce storage overhead. *ECT*'s role is to correct the model's mispredictions, in other words, the higher the model's accuracy, the smaller the *ECT*. Therefore, we have transformed the problem of reducing storage overhead into how to improve the model's accuracy.

Intuitively, increasing the model capacity infinitely can achieve 100% accuracy. However, like most systems [52], [53], DEHYDRATOR also faces the contradiction between performance and latency, and needs to complete the storage within an acceptable time. As shown in Section IV-F, we prove that the larger model is not always better. For a given provenance graph, there exists an  $\eta$ , such that when the model capacity is  $\eta$ , DEHYDRATOR achieves the maximum Latency-to-Storage Ratio. Although we have evaluated models of different capacities on different provenance graphs and proposed some strategies. However, due to the black-box nature of DNN, we are unable to theoretically derive the  $\eta$  for a given provenance graph. We will leave this work for the future.

DEHYDRATOR requires more time to store data than traditional database systems. However, this is acceptable since DEHYDRATOR is designed to store append-only provenance graphs, typically cold data. Due to its high overhead, it's important to note that DEHYDRATOR is not intended to be a general-purpose database. However, with advancements in AI acceleration techniques, DEHYDRATOR has the potential to evolve into a general graph database.

Unlike traditional databases, DEHYDRATOR does not ensure ACID (atomicity, consistency, isolation, durability) properties for a sequence of operations. DEHYDRATOR is designed for tasks that involve writing data once and reading it multiple times (cold storage), i.e., the provenance graph must remain unchanged to meet integrity requirements. Since there are no multiple writers, transaction support is unnecessary. We always validate the correctness and completeness of operations when writing to the database, ensuring that the returned results are accurate as long as execution integrity is upheld. DEHYDRATOR can also be adapted for other similar use cases.

## VI. RELATED WORK

**Intrusion Detection.** Existing provenance-based intrusion detection systems (PIDSeS) can be categorized as heuristic-based and anomaly-based. Heuristic-based PIDSeS [17], [18], [38], [43] use empirical knowledge based on MITRE ATT&CK's Tactics, Techniques, and Procedures (TTPs) [84] to construct matching rules to find known attacks in the provenance graph. HOLMES [17] develops graph-matching rules based on TTPs related to advanced persistent threat (APT) behavior. SLEUTH [38] designs a tag-based information flow propagation system that only alerts when certain confidentiality or integrity conditions are satisfied. Poirot [18] demonstrates that these event patterns can also be mapped from the graph extracted from Cyber Threat Intelligence (CTI) reports. However, they have difficulties in detecting unknown

attacks and extending scale. Anomaly-based PIDSeS detect intrusions by identifying deviations from normal behavior [78], [85], [41], [86], [85], [44], [87]. Streamspot [87] demonstrates a viable cluster-based modeling approach. Unicorn [86] visits each node to create a label to produce a histogram description of the graph which is then hashed into a fixed-length vector. The ShadeWatcher [78] and ThreaTrace [85] take a step in identifying anomalies at the node level but fail to reconstruct complete and coherent attack stories. KAIROS [41] leverages a novel graph neural network to learn the temporal evolution of the provenance graph's structural changes to quantify the degree of anomalousness for each event.

**Attack Investigation.** The attack investigation is to determine the source and scope of the attack, ascertain the extent of disruption, and develop remediation and prevention strategies. RapSheet [46] proposes a threat scoring scheme that evaluates the severity of each alert based on tactical provenance graphs (TPGs) to enable effective investigation of alerts. HERCULE [88] system correlates multi-source heterogeneous logs to construct a multi-dimensional weighted graph and uses the unsupervised community detection algorithm to discover attack-related paths from it. NODOZE [22] and PriorTracker [89] perform statistics on historical data and assign anomaly scores to events in the dependency graph. DEPIMPACT [48] calculates dependency weights globally based on multiple features and then aggregates the weights to nodes to determine suspicious points of intrusion. ATLAS [79] uses the combination of causal analysis, natural language processing, and machine learning to establish critical patterns of attack and non-attack behavior in the dependency graph. DEPCOMM [47] extracts summaries from each subgraph, enabling the generation of summary graphs from dependency graphs, thereby reducing the difficulty of investigation for analysts. WATSON [90] summarises the behavior of each node to infer the semantics of each audit event based on its context.

**Graph Compression.** Previous research has focused on developing methods to minimize log size while preserving critical forensic evidence. LogGC [28] employs graph analysis to identify and eliminate temporary file I/O and other "dead-end" activities, operating on the premise that events that do not contribute to the current state of the system are not useful for investigations. CPR [29] reduces redundant events between source and target nodes by examining *interleaved flows*, meaning whether any new inputs were received at the source between the two system calls. NodeMerge [30] is based on the observation that applications often load numerous globally read-only files at launch (e.g., shared object libraries), which can be consolidated. DPR [31] retains only the essential events required for accurately traversing each entity's ancestors (S-DPR) or both ancestors and successors (F-DPR), leading to a condensed provenance graph. *However, these techniques are lossy.* Xie et al. [91], [92], [93] suggest adaptations of web graph compression and dictionary encoding techniques for provenance graphs. Their approach involves applying web graph compression methods specifically to the context of provenance graphs. Fei et al. [37] implement the concept of Query-Friendly Compression from data mining in the realm of provenance graphs. ELISE [39] and Leonard [40]

integrate high-frequency field mapping encoding with deep neural networks to store provenance graphs efficiently.

## VII. CONCLUSION

In this paper, we propose a provenance graph storage system, DEHYDRATOR, which uses field-level mapping encoding and hierarchical encoding to filter field-level and structure-level redundancy, and utilizes DNN to support low-memory batch querying. Compared to existing databases, DEHYDRATOR achieves more efficient storage. Experimental results show that DEHYDRATOR reduces the storage space by 84.55%. In term of storage overhead, DEHYDRATOR is  $7.36 \times$  more efficient than PostgreSQL,  $7.16 \times$  than Neo4j, and  $16.17 \times$  than Leonard.

## REFERENCES

- [1] "Global data breaches and cyber attacks in 2024," 2024, <https://www.itgovernance.co.uk/blog/global-data-breaches-and-cyber-attacks-in-2024#top-stats>.
- [2] "Mother of all breaches reveals 26 billion records: what we know so far," 2024, <https://cybernews.com/security/billions-passwords-credentials-leaked-mother-of-all-breaches/>.
- [3] "India-linked hackers target pakistan with spyware in new campaign," 2024, <https://therecord.media/india-linked-hackers-target-pakistan-with-spyware>.
- [4] "Poland says russian cyberspies targeted government networks," 2024, <https://www.reuters.com/technology/cybersecurity/poland-says-it-was-targeted-by-hacking-attack-russia-linked-group-apt28-2024-05-08/>.
- [5] "Cyberattack on indonesia's national data centre paralyses government services," 2024, <https://govinsider.asia/intl-en/article/cyberattack-on-indonesias-national-data-centre-paraly-ses-government-services>.
- [6] "Groups," <https://attack.mitre.org/groups/>.
- [7] M. A. Inam, Y. Chen, A. Goyal, J. Liu, J. Mink, N. Michael, S. Gaur, A. Bates, and W. U. Hassan, "Sok: History is a vast early warning system: Auditing the provenance of system intrusions," in *2023 IEEE Symposium on Security and Privacy (SP)*. IEEE, 2023, pp. 2620–2638.
- [8] T. Jaeger, *Operating system security*. Springer Nature, 2022.
- [9] J. P. Anderson *et al.*, "Computer security technology planning study," Citeseer, Tech. Rep., 1972.
- [10] B. Lampson, "Perspectives on protection and security," in *SOSP History Day 2015*, ser. SOSP '15. New York, NY, USA: Association for Computing Machinery, 2015. [Online]. Available: <https://doi.org/10.1145/2830903.2830905>
- [11] Y. Zhai, P. Ning, and J. Xu, "Integrating ids alert correlation and os-level dependency tracking," in *Intelligence and Security Informatics: IEEE International Conference on Intelligence and Security Informatics, ISI 2006, San Diego, CA, USA, May 23-24, 2006. Proceedings 4*. Springer, 2006, pp. 272–284.
- [12] G. Gu, P. A. Porras, V. Yegneswaran, M. W. Fong, and W. Lee, "Bothunter: Detecting malware infection through ids-driven dialog correlation," in *USENIX Security Symposium*, vol. 7, 2007, pp. 1–16.
- [13] W. U. Hassan, D. Li, K. Jee, X. Yu, K. Zou, D. Wang, Z. Chen, Z. Li, J. Rhee, J. Gui *et al.*, "This is why we can't cache nice things: Lightning-fast threat hunting using suspicion-based hierarchical storage," in *Proceedings of the 36th Annual Computer Security Applications Conference*, 2020, pp. 165–178.
- [14] X. Chen, H. Irshad, Y. Chen, A. Gehani, and V. Yegneswaran, "[CLARION]: Sound and clear provenance tracking for microservice deployments," in *30th USENIX Security Symposium (USENIX Security 21)*, 2021, pp. 3989–4006.
- [15] P. Datta, I. Polinsky, M. A. Inam, A. Bates, and W. Enck, "[ALASTOR]: Reconstructing the provenance of serverless intrusions," in *31st USENIX Security Symposium (USENIX Security 22)*, 2022, pp. 2443–2460.
- [16] Z. Li, Q. A. Chen, R. Yang, Y. Chen, and W. Ruan, "Threat detection and investigation with system-level provenance graphs: A survey," *Computers & Security*, vol. 106, p. 102282, 2021.
- [17] S. M. Milajerdi, R. Gjomemo, B. Eshete, R. Sekar, and V. Venkatakrishnan, "Holmes: real-time apt detection through correlation of suspicious information flows," in *2019 IEEE Symposium on Security and Privacy (SP)*. IEEE, 2019, pp. 1137–1152.
- [18] S. M. Milajerdi, B. Eshete, R. Gjomemo, and V. Venkatakrishnan, "Poirot: Aligning attack behavior with kernel audit records for cyber threat hunting," in *Proceedings of the 2019 ACM SIGSAC conference on computer and communications security*, 2019, pp. 1795–1812.
- [19] Q. Wang, W. U. Hassan, D. Li, K. Jee, X. Yu, K. Zou, J. Rhee, Z. Chen, W. Cheng, C. A. Gunter *et al.*, "You are what you do: Hunting stealthy malware via data provenance analysis," in *NDSS*, 2020.
- [20] H. Irshad, G. Ciocarlie, A. Gehani, V. Yegneswaran, K. H. Lee, J. Patel, S. Jha, Y. Kwon, D. Xu, and X. Zhang, "Trace: Enterprise-wide provenance tracking for real-time apt detection," *IEEE Transactions on Information Forensics and Security*, vol. 16, pp. 4363–4376, 2021.
- [21] W. U. Hassan, A. Bates, and D. Marino, "Tactical provenance analysis for endpoint detection and response systems," in *2020 IEEE Symposium on Security and Privacy (SP)*. IEEE, 2020, pp. 1172–1189.
- [22] W. U. Hassan, S. Guo, D. Li, Z. Chen, K. Jee, Z. Li, and A. Bates, "Nodoze: Combatting threat alert fatigue with automated provenance triage," in *network and distributed systems security symposium*, 2019.
- [23] R. Aldeco-Pérez and L. Moreau, "Securing provenance-based audits," in *International Provenance and Annotation Workshop*. Springer, 2010, pp. 148–164.
- [24] C. Yagemann, M. A. Noureddine, W. U. Hassan, S. Chung, A. Bates, and W. Lee, "Validating the integrity of audit logs against execution repartitioning attacks," in *Proceedings of the 2021 ACM SIGSAC Conference on Computer and Communications Security*, 2021, pp. 3337–3351.
- [25] S. Ma, J. Zhai, Y. Kwon, K. H. Lee, X. Zhang, G. Ciocarlie, A. Gehani, V. Yegneswaran, D. Xu, and S. Jha, "{Kernel-Supported}{Cost-Effective} audit logging for causality tracking," in *2018 USENIX Annual Technical Conference (USENIX ATC 18)*, 2018, pp. 241–254.
- [26] A. Bates, D. J. Tian, K. R. Butler, and T. Moyer, "Trustworthy {Whole-System} provenance for the linux kernel," in *24th USENIX Security Symposium (USENIX Security 15)*, 2015, pp. 319–334.
- [27] Trustwave, "Trustwave global security report," 2015.
- [28] K. H. Lee, X. Zhang, and D. Xu, "Loggc: garbage collecting audit log," in *Proceedings of the 2013 ACM SIGSAC conference on Computer & communications security*, 2013, pp. 1005–1016.
- [29] Z. Xu, Z. Wu, Z. Li, K. Jee, J. Rhee, X. Xiao, F. Xu, H. Wang, and G. Jiang, "High fidelity data reduction for big data security dependency analyses," in *Proceedings of the 2016 ACM SIGSAC conference on computer and communications security*, 2016, pp. 504–516.
- [30] Y. Tang, D. Li, Z. Li, M. Zhang, K. Jee, X. Xiao, Z. Wu, J. Rhee, F. Xu, and Q. Li, "Nodemerger: Template based efficient data reduction for big-data causality analysis," in *Proceedings of the 2018 ACM SIGSAC Conference on Computer and Communications Security*, 2018, pp. 1324–1337.
- [31] M. N. Hossain, J. Wang, O. Weisse, R. Sekar, D. Genkin, B. He, S. D. Stoller, G. Fang, F. Piessens, E. Downing *et al.*, "{Dependence-Preserving} data compaction for scalable forensic analysis," in *27th USENIX Security Symposium (USENIX Security 18)*, 2018, pp. 1723–1740.
- [32] P. Deutsch, "Gzip file format specification version 4.3," Tech. Rep., 1996.
- [33] M. Goyal, K. Tatwawadi, S. Chandak, and I. Ochoa, "Deepzip: Lossless data compression using recurrent neural networks," *arXiv preprint arXiv:1811.08162*, 2018.
- [34] "Neo4j graph database," <https://neo4j.com/>.
- [35] "Orientdb," <https://orientdb.org/>.
- [36] "Titan graph database," <http://titan.thinkaurelius.com/>.
- [37] P. Fei, Z. Li, Z. Wang, X. Yu, D. Li, and K. Jee, "{SEAL}: Storage-efficient causality analysis on enterprise logs with query-friendly compression," in *30th USENIX Security Symposium (USENIX Security 21)*, 2021, pp. 2987–3004.
- [38] M. N. Hossain, S. M. Milajerdi, J. Wang, B. Eshete, R. Gjomemo, R. Sekar, S. Stoller, and V. Venkatakrishnan, "{SLEUTH}: Real-time attack scenario reconstruction from {COTS} audit data," in *26th USENIX Security Symposium (USENIX Security 17)*, 2017, pp. 487–504.
- [39] H. Ding, S. Yan, J. Zhai, and S. Ma, "{ELISE}: A storage efficient logging system powered by redundancy reduction and representation learning," in *30th USENIX Security Symposium (USENIX Security 21)*, 2021, pp. 3023–3040.
- [40] H. Ding, J. Zhai, D. Deng, and S. Ma, "The case for learned provenance graph storage systems," in *32nd USENIX Security Symposium (USENIX Security 23)*, 2023, pp. 3277–3294.
- [41] Z. Cheng, Q. Lv, J. Liang, Y. Wang, D. Sun, T. Pasquier, and X. Han, "Kairos: Practical intrusion detection and investigation using whole-system provenance," *arXiv preprint arXiv:2308.05034*, 2023.

- [42] S. T. King and P. M. Chen, "Backtracking intrusions," in *Proceedings of the nineteenth ACM symposium on Operating systems principles*, 2003, pp. 223–236.
- [43] T. Zhu, J. Yu, C. Xiong, W. Cheng, Q. Yuan, J. Ying, T. Chen, J. Zhang, M. Lv, Y. Chen *et al.*, "Aptshield: A stable, efficient and real-time apt detection system for linux hosts," *IEEE Transactions on Dependable and Secure Computing*, 2023.
- [44] F. Yang, J. Xu, C. Xiong, Z. Li, and K. Zhang, "{PROGRAPHER}: An anomaly detection system based on provenance graph embedding," in *32nd USENIX Security Symposium (USENIX Security 23)*, 2023, pp. 4355–4372.
- [45] "Darap3 transparent engagement 3," 2023, <https://drive.google.com/drive/folders/1QlbUFWAGq3Hpl8wVdzOdIoZLFxkII4EK>.
- [46] W. U. Hassan, A. Bates, and D. Marino, "Tactical provenance analysis for endpoint detection and response systems," in *2020 IEEE Symposium on Security and Privacy (SP)*. IEEE, 2020, pp. 1172–1189.
- [47] Z. Xu, P. Fang, C. Liu, X. Xiao, Y. Wen, and D. Meng, "Depcomm: Graph summarization on system audit logs for attack investigation," in *2022 IEEE Symposium on Security and Privacy (SP)*. IEEE, 2022, pp. 540–557.
- [48] P. Fang, P. Gao, C. Liu, E. Ayday, K. Jee, T. Wang, Y. F. Ye, Z. Liu, and X. Xiao, "{Back-Propagating} system dependency impact for attack investigation," in *31st USENIX Security Symposium (USENIX Security 22)*, 2022, pp. 2461–2478.
- [49] C. Xiong, T. Zhu, W. Dong, L. Ruan, R. Yang, Y. Cheng, Y. Chen, S. Cheng, and X. Chen, "Conan: A practical real-time apt detection system with high accuracy and efficiency," *IEEE Transactions on Dependable and Secure Computing*, vol. 19, no. 1, pp. 551–565, 2020.
- [50] M. N. Hossain, S. Sheikhi, and R. Sekar, "Combating dependence explosion in forensic analysis using alternative tag propagation semantics," in *2020 IEEE Symposium on Security and Privacy (SP)*. IEEE, 2020, pp. 1139–1155.
- [51] A. Ilkhechi, A. Crotty, A. Galakatos, Y. Mao, G. Fan, X. Shi, and U. Cetintemel, "Deepsqueeze: Deep semantic compression for tabular data," in *Proceedings of the 2020 ACM SIGMOD international conference on management of data*, 2020, pp. 1733–1746.
- [52] M. Stonebraker, D. J. Abadi, A. Batkin, X. Chen, M. Cherniack, M. Ferreira, E. Lau, A. Lin, S. Madden, E. O'Neil *et al.*, "C-store: a column-oriented dbms," in *Making Databases Work: the Pragmatic Wisdom of Michael Stonebraker*, 2018, pp. 491–518.
- [53] A. Lamb, M. Fuller, R. Varadarajan, N. Tran, B. Vandier, L. Doshi, and C. Bear, "The vertica analytic database: C-store 7 years later," *arXiv preprint arXiv:1208.4173*, 2012.
- [54] "Event tracing," <https://docs.microsoft.com/en-us/windows/desktop/ETW/event-tracing-portal>.
- [55] "System administration utilities," <https://man7.org/linux/man-pages/man8/auditd.8.html>.
- [56] "Dtrace on freebsd," <https://man7.org/linux/man-pages/man8/auditd.8.html>.
- [57] "The linux audit framework," 2017, <https://github.com/linux-audit/>.
- [58] Y. Bengio, R. Ducharme, and P. Vincent, "A neural probabilistic language model," *Advances in neural information processing systems*, vol. 13, 2000.
- [59] A. Vaswani, N. Shazeer, N. Parmar, J. Uszkoreit, L. Jones, A. N. Gomez, L. Kaiser, and I. Polosukhin, "Attention is all you need," *Advances in neural information processing systems*, vol. 30, 2017.
- [60] T. Mikolov, K. Chen, G. Corrado, and J. Dean, "Efficient estimation of word representations in vector space," *arXiv preprint arXiv:1301.3781*, 2013.
- [61] Z. Yang, Z. Dai, Y. Yang, J. Carbonell, R. R. Salakhutdinov, and Q. V. Le, "Xlnet: Generalized autoregressive pretraining for language understanding," *Advances in neural information processing systems*, vol. 32, 2019.
- [62] A. Radford, K. Narasimhan, T. Salimans, I. Sutskever *et al.*, "Improving language understanding by generative pre-training," 2018.
- [63] R. Socher, C. C. Lin, C. Manning, and A. Y. Ng, "Parsing natural scenes and natural language with recursive neural networks," in *Proceedings of the 28th international conference on machine learning (ICML-11)*, 2011, pp. 129–136.
- [64] S. Hochreiter and J. Schmidhuber, "Long short-term memory," *Neural computation*, vol. 9, no. 8, pp. 1735–1780, 1997.
- [65] J. Chung, C. Gulcehre, K. Cho, and Y. Bengio, "Empirical evaluation of gated recurrent neural networks on sequence modeling," *arXiv preprint arXiv:1412.3555*, 2014.
- [66] N. Bogoychev, "Not all parameters are born equal: Attention is mostly what you need," *arXiv preprint arXiv:2010.11859*, 2020.
- [67] J. Devlin, M.-W. Chang, K. Lee, and K. Toutanova, "Bert: Pre-training of deep bidirectional transformers for language understanding," *arXiv preprint arXiv:1810.04805*, 2018.
- [68] Y. Tay, M. Dehghani, S. Abnar, Y. Shen, D. Bahri, P. Pham, J. Rao, L. Yang, S. Ruder, and D. Metzler, "Long range arena: A benchmark for efficient transformers," *arXiv preprint arXiv:2011.04006*, 2020.
- [69] N. Shazeer, "Fast transformer decoding: One write-head is all you need," *arXiv preprint arXiv:1911.02150*, 2019.
- [70] K. Cao and M. Rei, "A joint model for word embedding and word morphology," *arXiv preprint arXiv:1606.02601*, 2016.
- [71] "Postgresql: The world's most advanced open source relational database," 2024, <https://www.postgresql.org/>.
- [72] A. Gehani and D. Tariq, "Spade: Support for provenance auditing in distributed environments," in *ACM/FIP/USENIX Int. Middleware Conf., MIDDLEWARE*. Springer, 2012, pp. 101–120.
- [73] "Sysdig," 2023, <https://github.com/draios/sysdig>.
- [74] "Postgresql copy command," 2024, <https://www.postgresql.org/docs/current/sql-copy.html>.
- [75] "Neo4j-admin import," 2024, <https://neo4j.com/docs/operations-manual/current/tutorial/neo4j-admin-import/>.
- [76] A. Jacot, F. Gabriel, and C. Hongler, "Neural tangent kernel: Convergence and generalization in neural networks," *Advances in neural information processing systems*, vol. 31, 2018.
- [77] Y. Lu, Z. Li, D. He, Z. Sun, B. Dong, T. Qin, L. Wang, and T.-Y. Liu, "Understanding and improving transformer from a multi-particle dynamic system point of view," *arXiv preprint arXiv:1906.02762*, 2019.
- [78] J. Zengy, X. Wang, J. Liu, Y. Chen, Z. Liang, T.-S. Chua, and Z. L. Chua, "Shadewatcher: Recommendation-guided cyber threat analysis using system audit records," in *2022 IEEE Symposium on Security and Privacy (SP)*. IEEE, 2022, pp. 489–506.
- [79] A. Alsaheel, Y. Nan, S. Ma, L. Yu, G. Walkup, Z. B. Celik, X. Zhang, and D. Xu, "{ATLAS}: A sequence-based learning approach for attack investigation," in *30th USENIX security symposium (USENIX security 21)*, 2021, pp. 3005–3022.
- [80] L. Kaiser, S. Bengio, A. Roy, A. Vaswani, N. Parmar, J. Uszkoreit, and N. Shazeer, "Fast decoding in sequence models using discrete latent variables," in *International Conference on Machine Learning*. PMLR, 2018, pp. 2390–2399.
- [81] M. Belkin, D. Hsu, S. Ma, and S. Mandal, "Reconciling modern machine-learning practice and the classical bias–variance trade-off," *Proceedings of the National Academy of Sciences*, vol. 116, no. 32, pp. 15 849–15 854, 2019.
- [82] M. Geiger, A. Jacot, S. Spigler, F. Gabriel, L. Sagun, S. d'Ascoli, G. Biroli, C. Hongler, and M. Wyart, "Scaling description of generalization with number of parameters in deep learning," *Journal of Statistical Mechanics: Theory and Experiment*, vol. 2020, no. 2, p. 023401, 2020.
- [83] P. Nakkiran, G. Kaplun, Y. Bansal, T. Yang, B. Barak, and I. Sutskever, "Deep double descent: Where bigger models and more data hurt," *Journal of Statistical Mechanics: Theory and Experiment*, vol. 2021, no. 12, p. 124003, 2021.
- [84] "Mitre attk," 2019, <https://attack.mitre.org>.
- [85] S. Wang, Z. Wang, T. Zhou, H. Sun, X. Yin, D. Han, H. Zhang, X. Shi, and J. Yang, "Threatrace: Detecting and tracing host-based threats in node level through provenance graph learning," *IEEE Transactions on Information Forensics and Security*, pp. 3972–3987, 2022.
- [86] X. Han, T. Pasquier, A. Bates, J. Mickens, and M. Seltzer, "Unicorn: Runtime provenance-based detector for advanced persistent threats," *arXiv preprint arXiv:2001.01525*, 2020.
- [87] E. Manzoor, S. M. Milajerdi, and L. Akoglu, "Fast memory-efficient anomaly detection in streaming heterogeneous graphs," in *Proceedings of the 22nd ACM SIGKDD International Conference on Knowledge Discovery and Data Mining*, 2016, p. 1035–1044. [Online]. Available: <https://doi.org/10.1145/2939672.2939783>
- [88] K. Pei *et al.*, "Hercule: Attack story reconstruction via community discovery on correlated log graph," in *ACSAC*, 2016, pp. 583–595.
- [89] Y. Liu *et al.*, "Towards a timely causality analysis for enterprise security," in *NDSS*, 2018.
- [90] J. Zeng *et al.*, "Watson: Abstracting behaviors from audit logs via aggregation of contextual semantics," in *NDSS*, 2021.
- [91] Y. Xie, K.-K. Muniswamy-Reddy, D. D. Long, A. Amer, D. Feng, and Z. Tan, "Compressing provenance graphs," in *3rd USENIX Workshop on the Theory and Practice of Provenance (TaPP 11)*, 2011.
- [92] Y. Xie, D. Feng, Z. Tan, L. Chen, K.-K. Muniswamy-Reddy, Y. Li, and D. D. Long, "A hybrid approach for efficient provenance storage," in *Proceedings of the 21st ACM international conference on Information and knowledge management*, 2012, pp. 1752–1756.

- [93] Y. Xie, K.-K. Muniswamy-Reddy, D. Feng, Y. Li, and D. D. Long, "Evaluation of a hybrid approach for efficient provenance storage," *ACM Transactions on Storage (TOS)*, vol. 9, no. 4, pp. 1–29, 2013.